

Density-controlled, solution-based growth of ZnO nanorod arrays via layer-by-layer polymer thin films for enhanced field emission

This article has been downloaded from IOPscience. Please scroll down to see the full text article.

2008 Nanotechnology 19 435302

(<http://iopscience.iop.org/0957-4484/19/43/435302>)

View [the table of contents for this issue](#), or go to the [journal homepage](#) for more

Download details:

IP Address: 130.207.50.192

The article was downloaded on 28/07/2010 at 15:56

Please note that [terms and conditions apply](#).

Density-controlled, solution-based growth of ZnO nanorod arrays via layer-by-layer polymer thin films for enhanced field emission

Benjamin Weintraub¹, Sehoon Chang², Srikanth Singamaneni²,
Won Hee Han³, Young Jin Choi⁴, Joonho Bae¹, Melanie Kirkham¹,
Vladimir V Tsukruk^{1,2} and Yulin Deng⁵

¹ School of Materials Science and Engineering, Georgia Institute of Technology, Atlanta, GA 30332-0245, USA

² School of Polymer, Textile and Fiber Engineering, Georgia Institute of Technology, Atlanta, GA 30332-0295, USA

³ Department of Physics, Myongji University, Yongin, Gyeonggi 449-728, Korea

⁴ Department of Nano Science and Engineering, Myongji University, Yongin, Gyeonggi 449-728, Korea

⁵ School of Chemical and Biomolecular Engineering, Georgia Institute of Technology, Atlanta, GA 30332-0620, USA

E-mail: yulin.deng@chbe.gatech.edu

Received 4 July 2008

Published 22 September 2008

Online at stacks.iop.org/Nano/19/435302

Abstract

A simple, scalable, and cost-effective technique for controlling the growth density of ZnO nanorod arrays based on a layer-by-layer polyelectrolyte polymer film is demonstrated. The ZnO nanorods were synthesized using a low temperature ($T = 90^\circ\text{C}$), solution-based method. The density-control technique utilizes a polymer thin film pre-coated on the substrate to control the mass transport of the reactant to the substrate. The density-controlled arrays were investigated as potential field emission candidates. The field emission results revealed that an emitter density of 7 nanorods μm^{-2} and a tapered nanorod morphology generated a high field enhancement factor of 5884. This novel technique shows promise for applications in flat panel display technology.

 Supplementary data are available from stacks.iop.org/Nano/19/435302

1. Introduction

Important for flat panel display technology, one-dimensional (1D) nanomaterials such as nanotubes and nanowires are considered promising candidates for achieving high field emission (FE) currents at low electric fields due to their high aspect ratios. In the last decade, FE research efforts have mostly focused on carbon nanotubes (CNTs) due to their high electrical conductivity, aspect ratio, thermal stability, and low fabrication cost [1–3]. However, metal oxide nanomaterials such as ZnO are attracting increasing interest because of their high chemical and thermal stability and tunable electronic properties. ZnO, a wide band-gap semiconductor ($E_g =$

3.37 eV) and piezoelectric material, is an important functional material used in photovoltaics, energy harvesting nanogenerators, and sensors [4–8].

For a given material, it has been shown that the FE efficiency can be improved by controlling the emitter density and aspect ratio [9–13]. Emitters that are too closely packed suffer from a screening effect, whereas emitters spaced too far apart approach the behavior of a thin film [11, 14]. Within the emitter density spectrum, there is an optimal density for achieving the best FE performance. In addition to optimizing emitter density, it has been shown that a sharp, elongated morphology such as a nano-needle or nano-pencil can improve FE performance [15, 16]. Because the field enhancement

factor β varies inversely with the radius of the emitter tip, a high local electric field can be generated at a sharp emitter tip to effectively lower the required FE potential barrier ($\beta = \text{emitter height/emitter tip radius}$).

Recently, Wang *et al* have developed a synthesis technique for controlling ZnO nanorod (NR) growth density and showed a correlation with field emission (FE) performance [14, 17]. However, this vapor–liquid–solid technique based on varying the thickness of a Au catalyst thin film requires a high temperature ($T = 950^\circ\text{C}$) to melt the Au catalyst, rendering it costly and incompatible with the organic materials valued in the flexible display industry. There has been little research into optimizing FE performance by controlling ZnO NR density using low temperature methods. Heralded for its low temperature compatibility with many organic materials, wet chemical ZnO nanowire synthesis based on the zinc nitrate/hexamethylenetetramine system is becoming quite popular due to its scalability and low cost, making it attractive for nano-manufacturing prospects [18]. Therefore, finding a technique to control NR growth density that is compatible with this technique is of great scientific and commercial interest.

With these considerations in mind, we developed a novel low temperature synthesis technique to control ZnO NR array density and morphology to optimize FE performance. Our approach was based on a low temperature, wet chemical ZnO NR synthesis technique using a ZnO thin film-deposited Si substrate. In general, ZnO NR array density is typically quite high when synthesized on a polycrystalline ZnO thin film, since each crystallite exposed to the nutrient solution can act as a growth site. Our idea was to establish a thin polymer film above the ZnO seed layer to inhibit precursor ion transport. In this way, the rate of reactant ions traveling from solution to the seed layer could be limited, thereby reducing the probability of eventual NR growth. Polyelectrolyte layer-by-layer (LBL) polymer thin films were chosen for this purpose because of their excellent thickness control and hydrophilic nature [19–21].

2. Experimental method

Si substrates with dimensions of $1\text{ cm} \times 1\text{ cm}$ were deposited with a 100 nm ZnO seed film by RF magnetron sputtering. To establish the ion transport barrier, the ZnO seed-coated samples were spin-coated with alternating layers of poly(allylamine hydrochloride) (PAH) and poly(sodium 4-styrenesulfonate) (PSS) polymers. Samples of 0, 1, 2, 3, 4, and 5 bilayers were prepared. Atomic force microscopy (AFM) analysis verified the film thicknesses and showed in general that each polymer bilayer measured 2.5 nm (see supplementary data S1, available at stacks.iop.org/Nano/19/435302). For solution-based NR array synthesis, the substrates were floated face-down in a 50 ml Pyrex glass bottle containing a 20 mM solution of zinc nitrate hexahydrate and hexamethylenetetramine (HMTA) and aged for 1.5 h at 90°C in a laboratory grade box oven. Substrates were subsequently rinsed with water and ethanol and oven dried at 60°C for 30 min in air.

All chemicals used were reagent grade. Zinc nitrate and hexamethylenetetramine were purchased from Fluka. PAH

and PSS purchased from Sigma-Aldrich had a M_w of 70 000 and a concentration of 0.2% (w/w). Details of the LBL deposition process can be found elsewhere [28, 29]. Substrates of (100) oriented Si were sputtered at room temperature and then annealed at 350°C for 20 min to improve grain alignment and crystallinity. NR characterization was carried out on a LEO 1530 FE scanning electron microscope (SEM) operated at 5 kV. X-ray diffraction data were collected on a Panalytical X'Pert Pro diffractometer with Cu $K\alpha$ radiation.

AFM topographical and phase images (see supplementary data S1, available at stacks.iop.org/Nano/19/435302) were collected on a Digital Instruments Dimension 3000 in tapping mode under ambient conditions. For these measurements, LBL polymers were spin-coated onto bare Si substrates to minimize the effects of surface roughness. The thickness of the polymer layers with different numbers of bilayers was measured using AFM by scanning along the edge of the film. For FE measurements, a Keithley 6517A electrometer was used to both apply the voltage and measure the current. Fluorescence images were taken on a Canon 400D camera fitted with a EF50 mm f/2.5 compact macro lens.

3. Results and discussion

3.1. Structural analysis of density-controlled nanorod arrays

Figure 1 displays the representative SEM images of the density-controlled ZnO NR arrays for the 0, 1, 3, and 5 bilayer samples showing the general trend of decreasing density. As expected in figure 1(a), the sample without a polymer barrier exhibits the highest density. Likewise, the density decreases as the number of polymer bilayers increases, as shown in figures 1(b)–(d) corresponding to 1, 3, and 5 bilayer samples, respectively. The insets in figure 1 show high magnification SEM images of the morphology. It can be seen that the NRs become tapered for the polymer-coated samples. We believe that the polymer layer effectively slowed the initial NR growth kinetics. As the polymer layer increased to 5 layers (figure 1(d)), instead of NR growth some ZnO particles precipitated out in the solution. As the reaction sequence proceeds, the available ZnO precursor ions begin to decrease and the net effect is a morphological NR tapering. The rod size and length distributions were also increased when the number of the polymer thin layers was increased.

Quantitative analysis was carried out to determine the relationship between both the NR density and the tip diameter and the number of polymer bilayers, as shown in figure 2(a). The density was uniform throughout the $1\text{ cm} \times 1\text{ cm}$ substrate. The average NR density was calculated by counting the number of NRs shown in SEM images of the same magnification at three different substrate locations chosen at random. As shown in figure 2(a), the average NR density decreases exponentially with values of 123, 48, 11, 7, 2, and 1 NR μm^{-2} corresponding to 0, 1, 2, 3, 4, and 5 polymer bilayers. It should be noted that the FE performance strongly depends on the tip diameter. The average NR tip diameter, estimated by measuring the tip diameter of 20 NRs chosen at random and imaged using high magnification SEM, indicates

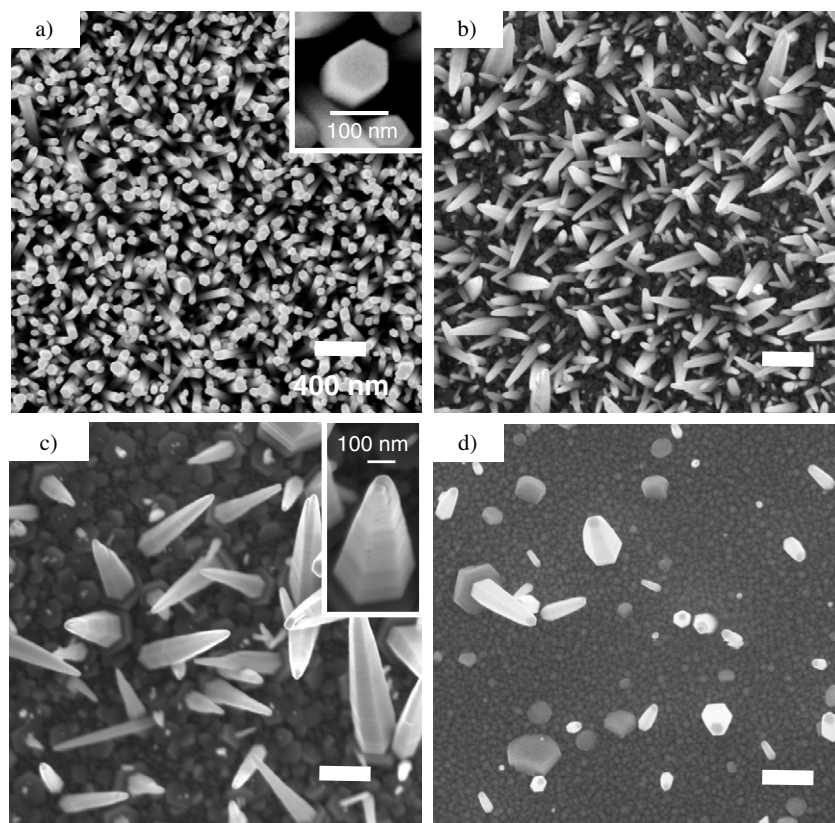


Figure 1. Top view: SEM micrographs, at the same magnification, of ZnO nanorod arrays with substrates having a varying number of PSS/PAS bilayers: (a) 0 bilayers (inset shows nanorod morphology); (b) 1 bilayer; (c) 3 bilayers (inset shows nanorod morphology); (d) 5 bilayers.

that although the base diameter increased, the change in tip diameter is not significant, as shown in figure 2(a). NRs in the various samples ranged in length from about 0.2 to 2 μm .

The x-ray diffraction data shown in figure 2(b) confirm the epitaxial nature of the aligned NRs with the seeds as well as the (001) fast growth direction. The two strong peaks seen at 33.0° and 34.4° correspond to the substrate Si(200) and ZnO(002) planes. The presence of only a single ZnO(002) peak indicates a high degree of vertical alignment. Weak peaks at 31.8° and 36.3°, present only in the case of the sample with 5 bilayers, correspond to ZnO(100) and ZnO(101) reflections and indicate that this sample had poor vertical alignment.

AFM analysis (see supplementary data S1, available at stacks.iop.org/Nano/19/435302) revealed that the samples with 1 and 2 polymer bilayers with thicknesses of 2.5 and 5.0 nm, respectively, contained small penetrating pores which directly exposed the ZnO seed layer to the nutrient solution. Thus, the density of the pores most likely controlled the ion transport to the seed layer. In the samples with 3, 4, and 5 bilayers corresponding to thicknesses of 7.5, 10, and 12.5 nm, respectively, the AFM results show that the polymer film did not contain any penetrating pores and fully covered the seed layer. It is believed that the hydrophilic PAH/PSS LBL polymer swelled in the aqueous solution allowing for the passage of ZnO intermediate precursor ions such as $\text{Zn}(\text{OH})_4^{2-}$ and $\text{Zn}(\text{NH}_3)_4^{2+}$ [22]. In this case, the thickness of the polymer

primarily controlled the ion transport to the seed layer surface and the probability of eventual NR growth.

3.2. Patterned growth of density-controlled nanorod arrays

To reliably incorporate ZnO NR arrays into electronic device applications it is important to achieve scalability and process control. To demonstrate the precise level of density control possible using this technique, patterned substrates of varying density were prepared using soft lithography methods over an area of 1 mm \times 1 mm. The SEM images can be seen in figure 3. Regions of varying polymer thickness were patterned corresponding to 3 and 13 bilayer stripes on a ZnO thin film-deposited Si substrate. A simple process flow was employed, shown in figure 3(a), based on capillary transfer lithography. First, the ZnO thin film was coated with 3 bilayers of PAH/PSS. Second, a 400 nm thick polystyrene (PS) pattern with a periodicity of 10 μm defined by a polydimethylsiloxane (PDMS) stamp was deposited onto the initial 3 bilayers. Next, an additional 10 PAH/PSS bilayers were spin-coated on top of the PS patterned substrate to provide a thickness differential. Finally, the PS pattern was lifted off in toluene leaving patterned stripe features with 3 and 13 bilayers on the ZnO seed layer. After patterning, the substrates were subjected to the same solution-based synthesis conditions as described above. The stripes can be seen in the low magnification top view SEM image in figure 3(b). Figure 3(c) shows the thinner

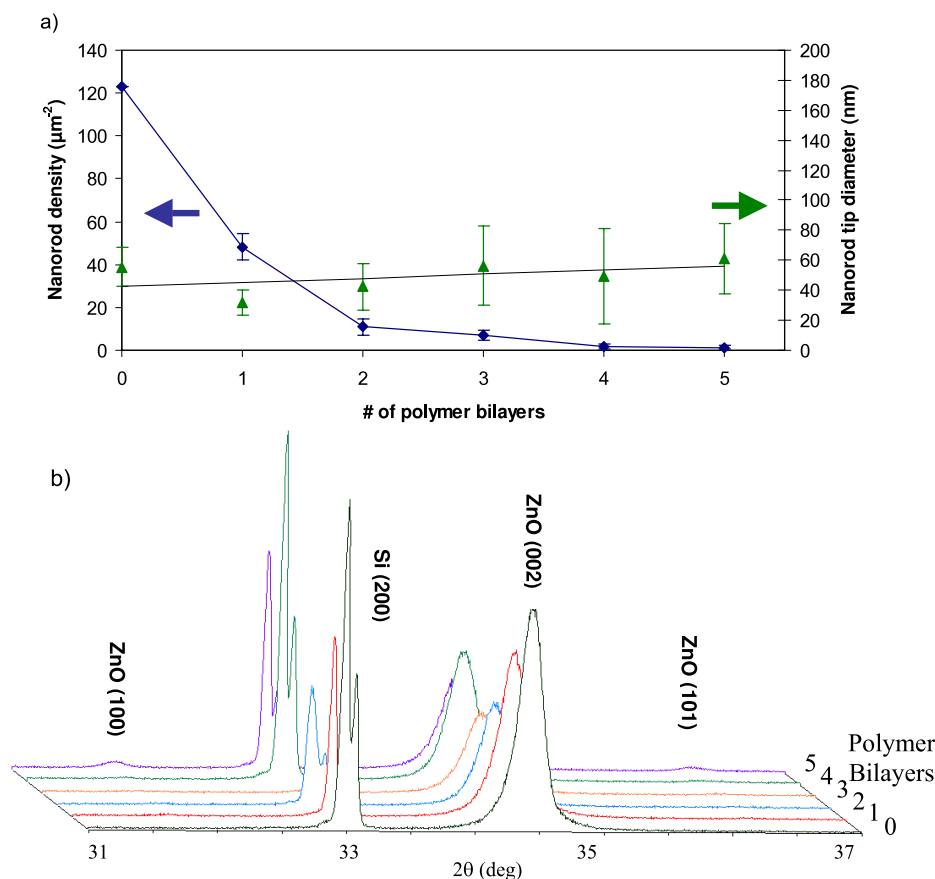


Figure 2. (a) Plot of nanorod density and nanorod tip diameter as a function of the number of LBL polymer bilayers. (b) X-ray diffraction spectra for the samples with differing numbers of polymer bilayers.

(This figure is in colour only in the electronic version)

3-bilayer $7 \mu\text{m}$ wide stripe regions exhibiting a higher NR density than the thicker 13-bilayer $3 \mu\text{m}$ wide stripe regions. The 60° tilted SEM image in figure 3(d) further reveals the disparity in growth density. This evidence further supports the idea that polymer thickness controls the NR growth density.

A differential thickness of about 8 nm verified by AFM was significantly smaller than that expected for 10 bilayers (about 23 nm). This can be explained by the presence of hydrophobic PS stripes on the initial 3 bilayers causing the surface to wet poorly with the subsequent hydrophilic polymer solution. Furthermore, the force exerted during the PDMS stamping process caused compression of the initial 3 bilayers, verified by AFM. While it seems unlikely that the elastomeric PDMS stamp could cause sufficient stress to deform a glassy LBL polymer, a significant depression in T_g for an ultrathin polymer film may occur [23, 24]. Due to the ultrathin nature of the film, the initial 3 bilayers (about 7.5 nm) exhibited a relatively low stiffness, resulting in compression during the stamping process. All these factors likely contributed to the lower than expected polymer thickness differential.

3.3. Field emission properties

To investigate the influence of NR array density on FE properties, representative samples of 0, 1, 3, and 5 bilayers

were tested using a simple diode configuration. A gap distance of about $80 \mu\text{m}$ was fixed between an ITO glass anode and the NR array cathode by Kapton and Si spacers. The vacuum level of the measurement chamber was maintained at 1×10^{-6} Torr. Figure 4(a) shows the results for measurements of current density versus applied electric field for the series of samples. Similar to CNTs, the highest density 0-bilayer sample performed poorly as a field emitter; this is generally attributed to a screening effect [11]. The turn-on field was $14.1 \text{ V } \mu\text{m}^{-1}$ at a current density of $10 \mu\text{A cm}^{-2}$. The FE data reveal that the medium density 1- and 3-bilayer samples showed the best FE performance. They turned on at electric fields of 9.8 and $5.1 \text{ V } \mu\text{m}^{-1}$, respectively. The 3-bilayer sample jumped to a high current density of $50 \mu\text{A cm}^{-2}$ at an electric field of about $7 \text{ V } \mu\text{m}^{-1}$. The lowest density sample of 5 bilayers showed poor FE efficiency as it did not draw a current density above $10 \mu\text{A cm}^{-2}$. This density versus FE performance trend is consistent with others [14]. The values of the turn-on field are summarized in table 1. The inset in figure 4(a) shows a representative fluorescence image for the medium density samples. This fluorescence image of the 1-bilayer sample at an electric field of $62.5 \text{ V } \mu\text{m}^{-1}$ demonstrates a relatively uniform emission over a large sample surface area.

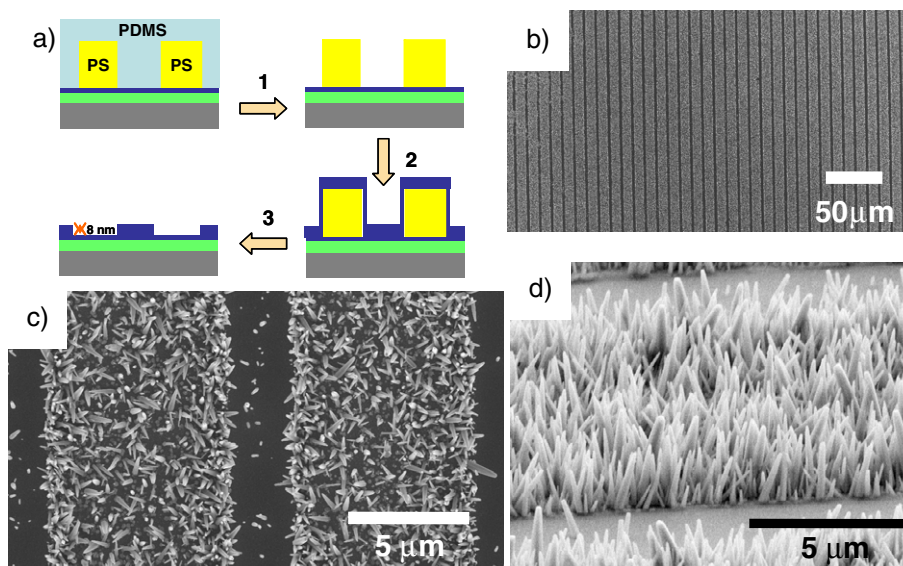


Figure 3. Patterned growth via microcontact printing. (a) Process flow for soft lithography (not to scale). A ZnO-coated Si substrate contains an initial 3 PSS/PAH bilayers. In step 1, a polystyrene (PS) stripe pattern is transferred to the substrate. In step 2, an additional 10 bilayers is spin-coated. In step 3, the PS is dissolved leaving an 8 nm differential thickness. (b) Low magnification SEM image of a striped pattern of bilayers with a 10 μm periodicity. (c) High magnification SEM image of a stripe pattern. (d) 60° tilted SEM image of a patterned sample.

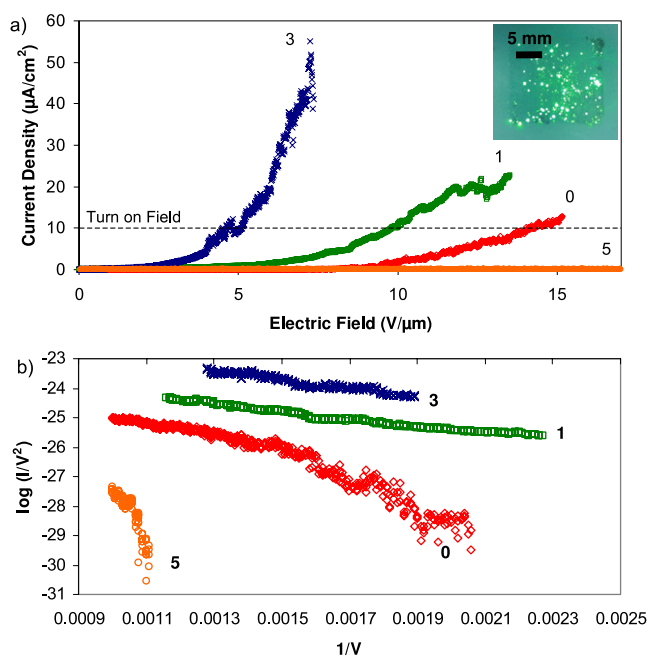


Figure 4. Field emission data: (a) field emission I - V data for samples with 0, 1, 3, and 5 bilayers. The inset shows a fluorescence image of the 1-bilayer sample. (b) Fowler-Nordheim plots.

The current-voltage (I - V) plots were converted to Fowler-Nordheim (F-N) plots by expressing $\ln(I/V^2)$ versus $1/V$ and are shown in figure 4(b). The four F-N curves show a linear behavior and negative slope, indicating that the FE current originates from barrier tunneling from the cathode due to an electric field. The field enhancement factor β , describing the ratio of the local electric field at the emitter tip versus the macroscopic electric field, can be calculated from the

Table 1. Summary of field enhancement factors and turn-on fields for ZnO NR arrays of different densities.

Number of polymer bilayers	NR density (μm^{-2})	β	E_{TO} ($\text{V } \mu\text{m}^{-1}$)
0	123	1538	14.1
1	48	4910	9.8
3	7	5884	5.1
5	1	173	N/A

F-N curve slope according to

$$\beta = 6.83 \times 10^9 \frac{d\phi^{3/2}}{k}, \quad (1)$$

where d is the gap distance, ϕ is the work function of ZnO (5.2 eV) and k is the slope of the F-N curve. Following a trend similar to the turn-on field, NR samples with 1 and 3 bilayers show the highest field enhancement factors of 4910 and 5884, respectively. Table 1 summarizes the field enhancement factors. In general, a wide range of β values have been reported in the literature for ZnO nanostructures ranging from about 300 to 41 000 [25]. The highest values have been achieved using high temperature synthesis techniques such as carbothermal vapor transport, molten-salt-assisted thermal evaporation, and metal organic chemical vapor deposition [10, 15, 26]. In terms of low temperature, solution-based FE studies, Liu *et al* and Ahsanulhaq *et al* have recently reported β values of 2350 and 1680, respectively [16, 27]. Our high reported value of 5884 is generally attributed to the optimized density and tapered morphology giving rise to a sharp emitter tip with a large localized electric field. Thus, this reasonably large β value of 5884 along with the low turn-on field of 5.1 $\text{V } \mu\text{m}^{-1}$ achieved in the 3-bilayer sample suggest that the decreased NR density and tapered morphology could be useful to fabricate optimized ZnO field emitters.

4. Conclusions

In summary, a simple, scalable, and cost-effective technique for controlling the growth density of ZnO NR arrays by varying polymer film thickness has been demonstrated. The FE results revealed that an emitter density of $7 \mu\text{m}^{-2}$ and a tapered NR morphology resulted in a high field enhancement factor of 5884, making this an important technique for flat panel display technology. Lastly, this low temperature technique can easily be extended to organic substrates for FE devices based on flexible electronic NR arrays, such as electronic paper.

Acknowledgments

BW thanks IPST at Georgia Tech for the fellowship. YJC acknowledges the grant from the Center for Nanoscale Mechatronics & Manufacturing, one of the 21st Century Frontier Research Programs, supported by the Ministry of Education, Science and Technology, Korea.

References

- [1] Milne W I, Teo K B K, Amaratunga G A J, Legagneux P, Gangloff L, Schnell J P, Semet V, Binh V T and Groening O 2004 *J. Mater. Chem.* **14** 933–43
- [2] Bai X, Wang M S, Zhang G M, Yu J, Zhang Z X, Guo D Z, Zhao X Y and Xue Z Q 2007 *J. Vac. Sci. Technol. B* **25** 561–5
- [3] Deheer W A, Chatelain A and Ugarte D 1995 *Science* **270** 1179–80
- [4] Qin Y, Wang X D and Wang Z L 2008 *Nature* **451** 809–13
- [5] Wang X D, Song J H, Liu J and Wang Z L 2007 *Science* **316** 102–5
- [6] Wang Z L and Song J H 2006 *Science* **312** 242–6
- [7] Huang M H, Mao S, Feick H, Yan H Q, Wu Y Y, Kind H, Weber E, Russo R and Yang P D 2001 *Science* **292** 1897–9
- [8] Law M, Greene L E, Johnson J C, Saykally R and Yang P D 2005 *Nat. Mater.* **4** 455–9
- [9] Li X J and Jiang W F 2007 *Nanotechnology* **18** 065203
- [10] Banerjee D, Jo S H and Ren Z F 2004 *Adv. Mater.* **16** 2028–32
- [11] Nilsson L, Groening O, Emmenegger C, Kuettel O, Schaller E, Schlappbach L, Kind H, Bonard J M and Kern K 2000 *Appl. Phys. Lett.* **76** 2071–3
- [12] Bonard J M, Weiss N, Kind H, Stockli T, Forro L, Kern K and Chatelain A 2001 *Adv. Mater.* **13** 184–8
- [13] Teo K B K, Chhowalla M, Amaratunga G A J, Milne W I, Pirio G, Legagneux P, Wyczisk F, Pribat D and Hasko D G 2002 *Appl. Phys. Lett.* **80** 2011–3
- [14] Wang X D, Zhou J, Lao C S, Song J H, Xu N S and Wang Z L 2007 *Adv. Mater.* **19** 1627–31
- [15] Park C J, Choi D K, Yoo J, Yi G C and Lee C J 2007 *Appl. Phys. Lett.* **90** 83107
- [16] Liu J P, Huang X T, Li Y Y, Ji X X, Li Z K, He X and Sun F L 2007 *J. Phys. Chem. C* **111** 4990–7
- [17] Wang X D, Song J H, Summers C J, Ryou J H, Li P, Dupuis R D and Wang Z L 2006 *J. Phys. Chem. B* **110** 7720–4
- [18] Vayssieres L 2003 *Adv. Mater.* **15** 464–6
- [19] Tang Z Y, Wang Y, Podsiadlo P and Kotov N A 2006 *Adv. Mater.* **18** 3203–24
- [20] Decher G, Hong J D and Schmitt J 1992 *Thin Solid Films* **210** 831–5
- [21] Jiang C Y, Markutsya S, Pikus Y and Tsukruk V V 2004 *Nat. Mater.* **3** 721–8
- [22] Govender K, Boyle D S, Kenway P B and O'Brien P 2004 *J. Mater. Chem.* **14** 2575–91
- [23] Forrest J A, Dalnoki-Veress K and Dutcher J R 1997 *Phys. Rev. E* **56** 5705–16
- [24] Gorbunov V V, Fuchigami N and Tsukruk V V 2000 *High Perform. Polym.* **12** 603–10
- [25] Fang X, Bando Y, Gautam U K, Ye C and Golberg D 2008 *J. Mater. Chem.* **18** 509–22
- [26] Wang W Z, Zeng B Q, Yang J, Poudel B, Huang J Y, Naughton M J and Ren Z F 2006 *Adv. Mater.* **18** 3275–9
- [27] Ahsanulhaq Q, Kim J H and Hahn Y B 2007 *Nanotechnology* **18** 485307
- [28] Jiang C Y, Markutsya S and Tsukruk V V 2004 *Langmuir* **20** 882–90
- [29] Jiang C Y, Markutsya S and Tsukruk V V 2004 *Adv. Mater.* **16** 157–61